Investigations of Spot-to-plume Mode Transition in a Hollow Cathode Discharge Using 2-D Axisymmetric Plasma Simulations

Ioannis G. Mikellides,[*] Pablo Guerrero,[†] Alejandro Lopez Ortega,[‡]
Dan M. Goebel[§] and James E. Polk[**]
Jet Propulsion Laboratory, California Institute of Technology, Pasadena, CA, 91109

Abstract: After decades of laboratory investigations that provided invaluable measurements and insight, the physics behind the transition from spot to plume modes in hollow cathodes remains one of the longest standing theoretical problems in electric propulsion. This has prohibited the development of *ab initio* models that allow for the prediction of the transition across different cathodes and operating conditions. Since the beginning of its development over a decade ago, simulations with the 2-D axisymmetric Orificed Cathode (OrCa2D) code have helped elucidate a wide range of processes in hollow cathode discharges. However, the code has never been used to investigate the onset of plume mode. We present results from the first OrCa2D simulations of a 25-A LaB_6 cathode for a range of flow rates (5-20 sccm) in which transition from spot to plume modes is known to occur. The cathode in this study was one of the two technologies considered for the 12.5 kW Hall Effect Rocket with Magnetic Shielding (HERMeS) and operates nominally at 21 A and 14.8 sccm. The simulations capture the characteristic rise of the peak-to-peak amplitude in the keeper voltage oscillations and underscore the significance of the plume neutral gas in the transition. The plasma inside the cathode is found to be relatively quiescent throughout the transition, in agreement with previous experimental observations. The computed keeper voltage fluctuations at low flow rates (<8 sccm) are found to be driven by oscillations of the same frequency in the plasma plume with the following main characteristics: (1) they are of low frequency (<10 kHz), and associated with small longitudinal motion in the direction of the applied magnetic field, (2) they occur in a region of the plume where the neutral gas provided by the cathode has been fully depleted, and (3) they have a (small) wave velocity of about 100 m/s, which is at least ~10× smaller than the drift, thermal and acoustic speeds of the ions. At 8 sccm, when the transition to the large-amplitude oscillations begins, the ionization frequency in the neutral-depleted plume region ranges ~2-100 kHz. The frequency of the oscillations in the plasma (and keeper voltage) is found to be equal to the ionization frequency (~5 kHz) at the center of this region. The findings suggest that the transition to plume mode is driven by ionization processes in the near-plume of the cathode, in line with previous conjectures that were based solely on laboratory observations.

[*]Principal Engineer, Electric Propulsion Group, Jet Propulsion Laboratory, California Institute of Technology, M/S 125-109, 4800 Oak Grove Drive, Pasadena, CA 91109. Associate Fellow AIAA.
[†]PhD Candidate, Galcit, California Institute of Technology, 1200 E California Blvd, Pasadena, CA 91125. Student Member AIAA.
[‡]Member of the Technical Staff, Electric Propulsion Group, Jet Propulsion Laboratory, California Institute of Technology, M/S 125-109, 4800 Oak Grove Drive, Pasadena, CA 91109. Member AIAA.
[§]Senior Research Scientist, Propulsion and Materials Engineering Section, Jet Propulsion Laboratory, California Institute of Technology, M/S 125-109, 4800 Oak Grove Drive, Pasadena, CA 91109. Fellow AIAA.
[**]Principal Engineer, Propulsion and Materials Engineering Section, Jet Propulsion Laboratory, California Institute of Technology, M/S 125-109, 4800 Oak Grove Drive, Pasadena, CA 91109. Associate Fellow AIAA.

© 2018. California Institute of Technology. Government sponsorship acknowledged.

I. Introduction

It has been known for decades that the discharge in electric propulsion hollow cathodes exhibits distinct dynamic behavior under different operating conditions. During investigations of a neutralizer hollow cathode operating with mercury in the late 1960's, Rawlin and Pawlik [1] observed that when the cathode was operated at high enough flow rates the oscilloscope traces were free of noise and that only a "small spot" of plasma was visible at the orifice. Hence, they termed this mode of operation "spot mode." As the flow rate was lowered, the authors observed a more pronounced "plume of plasma" that extended from the orifice to the beam simulator electrode. When the flow rates were low enough both keeper and anode voltage traces yielded appreciable level of noise. Shortly thereafter Csiky [2] made similar observations about operation in this mode, now known as "plume mode," in a mercury cathode of the type used in the SERT II ion engines.

Since then there have been extensive investigations of these two modes due largely to their implications on thruster stability and life. More specifically, when in plume mode, surges in both the keeper voltage [1-5] and the keeper wear are known to occur [6, 7]. Naturally then the questions of what conditions allow a cathode of a given geometry to operate in the (favorable) spot mode, how and why it transitions to the (unfavorable) plume mode, and what are the driving physics behind the two modes, have served as the impetus behind most investigations since those early studies in the late 60s. The majority of the investigations on the two modes have been experimental. A detailed review of the voluminous material that exists in the literature on this topic is beyond the scope of this article. However, we provide in this section a brief summary of the main findings to help illustrate the motivation and purpose of the work reported here. For a more detailed review the reader is referred to Goebel and Katz [8] and references therein.

In general, transition to plume mode occurs when the ratio of discharge current to mass flow rate ($I_d/\dot{m}$) exceeds some value that is dependent, among others, on the applied magnetic field and cathode geometry. More specifically, in ion engine neutralizer hollow cathodes transition from spot to plume mode occurs when the propellant flow rate and/or keeper current become exceedingly low for a given cathode geometry and desired beam current. When in plume mode, oscillations in the keeper or coupling voltage increase. For example, the onset of plume mode was defined to occur in the neutralizer cathode of the NASA Solar Technology Application Readiness (NSTAR) ion engine when the peak-to-peak keeper voltage oscillation exceeded 5 V [9]. As such, cathodes in electric propulsion are designed to operate at oscillation levels considerably lower than that, namely in spot mode. In discharge cathodes, plume mode also occurs when the discharge current becomes exceedingly high for a given flow rate, and is usually manifested as an increase in the discharge voltage oscillations.

It has been argued that plume mode is driven by ionization oscillations in the near plume of the hollow cathode. For example, Goebel, *et al*. [10] reported probe measurements that revealed only small-amplitude density fluctuations of the plasma inside a 25-A discharge cathode during plume-mode operation. By contrast, the authors measured large-amplitude oscillations in the plume region near the keeper. These oscillations were uncorrelated to those measured inside. Moreover, using measured density and electron temperature measurements in the near plume and by assuming a degree of ionization there, they found that the ionization frequency at a location in the plume where the plasma was most luminous was comparable to the frequency of the measured oscillations in the plasma (~80 kHz). This supported the argument that there is at least a correlation between ionization and the observed oscillations [10]. Further evidence that plume mode may be associated with ionization processes in the cathode plume is that its transition from spot mode is affected by the anode location and design [11], arguably because it can alter the gas density and, in turn, the plasma generation rate in this region [8, 12]. During a parametric investigation of a 100-A LaB_6 cathode, Jorns, *et al*. [13] measured ion acoustic turbulence (IAT) in the discharge plume in the frequency range of 400-1000 kHz. The IAT was present at all ratios $I_d/\dot{m}$ but the wave amplitude at first decreased and then increased with discharge current at fixed flow rate; it decreased with flow rate at fixed discharge current. At almost all discharge currents they also measured a distinct low-frequency peak in the spectra, 50-100 kHz, which corresponded to a dispersion-less mode. The authors hypothesized that this mode was likely associated with a coherent ionization instability. The ionization oscillations were dominant

enough at these low frequencies that it became difficult to distinguish the IAT, especially at low discharge currents.

The breadth of laboratory investigations that have taken place on this topic since the 60's was never matched by theoretical studies, probably due to the inherent theoretical complexity of the problem and the lack of numerical simulation capabilities beyond zeroth and one dimensions. It is possible that the robustness of these devices, and the ease with which the operational range of spot and plume modes (the so-called plume-mode margin) can be measured in the laboratory, also contributed to the lack of progress in the modeling and simulation of this problem. Some of the earliest first-principles models of hollow cathodes were in fact in 0-D (e.g. see [14] and [15]). For example, in the mid-90s Mandel and Katz [15] postulated that the transition between plume and spot modes in a plasma contactor is associated with the sheath that forms around the keeper and its ability to collect the discharge current from the generated plasma. More recently, by performing a linear perturbation analysis of the equations of motion for the plasma to obtain a dispersion relation, Georgin and Jorns [16] argued that plume mode is driven by the onset of IAT. IAT is now known to exist in hollow cathode plumes, as theoretically predicted by Mikellides, *et al*. [17] and later experimentally confirmed by Jorns, *et al*. [13]. In the time that transpired between these two studies many different models of the hollow cathode were developed, mostly in 0-D and 1-D. The vast majority of the models however did not address the physics behind the transition from spot to plume mode. A noteworthy exception is the recent work by Sary and Garrigues [18] who developed a 2-D axisymmetric model of the discharge in these devices. This work followed on the footsteps of OrCa2D (Orifice Cathode in 2-D) developed at the Jet Propulsion Laboratory in the mid-2000s, the first model of its kind to allow for numerical simulations of the cathode discharge in a 2-D axisymmetric domain that spans both the cathode interior and plume regions [19-22]. After simulating an NSTAR-like discharge hollow cathode in the absence of an applied magnetic field, Sary & Garrigues found no ionization instability in the near plume. However, at ratios of $I_d/\dot{m}$ they computed fluctuations in the plasma potential with larger than measured amplitudes (tens of volts) at the keeper exit plane and anode. They attributed these oscillations to the growth of the IAT [18].

OrCa2D has never been employed to investigate the reasons and the manner in which the cathode discharge transitions from spot to plume mode, until now. The motivation for this work is related to operation of the hollow cathode in a Hall thruster, which differs from that in ion engines, both in terms of how the discharge couples to the thruster plasma and where the anode is located relative to the cathode. Typically, the nominal flow rates in Hall thruster cathodes are much higher than those in ion engines for the same discharge current. Therefore, operation in plume mode is not a major concern. Nevertheless, if ionization in the plume is indeed the driver behind the transition then the neutral gas in this region must play a significant role. A few questions then naturally arise: (1) how does the location of the cathode discharge relative to the Hall thruster plume affect the transition, (2) is the determination of the plume margin from a stand-alone cathode test that uses a different anode arrangement than that in the thruster, truly "similar" and, (3) what are the effects of facility backpressure on the transition? If plume ionization is not the driver of the oscillations but some other instability (or instabilities) is, what excites it, how does it couple to the anomalous transport that is known to exist in Hall thrusters and, does it have any implications on the production of (cathode) high-energy ions that can enhance erosion of the thruster poles? It is noted here that at sufficiently high discharge currents the IAT is known to produce high-energy ions in the cathode plume [21, 23].

These questions have immediate impact on the ongoing work with the 12.5-kW Hall Effect Rocket with Magnetic Shielding (HERMeS) [24, 25] at the NASA Glenn Research Center (GRC) and the Jet Propulsion Laboratory (JPL). HERMeS is part of the Ion Propulsion System under development through the Advanced Electric Propulsion System contract with Aerojet Rocketdyne [26]. The work at the two centers aims to support thruster tests, risk reduction and life qualification activities while also providing oversight of the contract. The thruster is operated at a nominal discharge current and voltage of 20.8 A and 300-600 V, respectively, and uses a centrally mounted cathode. Two cathode technologies were considered for HERMeS that are distinguished mainly by the emitter material they employ, Lanthanum hexaboride (LaB_6) or Barium Oxide (BaO). Before the recent selection of the BaO cathode as the baseline for HERMeS,

prototypes of both cathodes were developed and tested. We have used in our simulations the LaB_6 prototype largely because of readily available data from characterization tests at JPL.

A description of the cathode arrangement and the experiments that produced the measurements we have used for model validation and guidance are provided in Sec. II. Section III describes the computational domain and main features of OrCa2D. The results from the investigations are reported in Sec. IV. The section includes also comparisons with plasma measurements and data from cathode characterizations tests. The article concludes with Sec. V.

II. The Hollow Cathode Experiments

Two cathode technologies were considered for HERMeS, distinguished mainly by the emitter material they employed (LaB_6 or BaO). Before the recent selection of the BaO cathode as the baseline for this thruster, prototypes of both cathodes were developed and tested. In the present investigation we have used data from tests of two identical versions of the LaB_6 prototype cathode called Test Development Units-1 and -2 (TDU-1 and TDU-2). The cathodes and wear tests were described in detail by Goebel, *et al*. in [27]. Here, for completeness, we provide a brief summary of the information that is most relevant to our investigations.

The cathode unit has an outer diameter of 1.3 cm and was previously labeled as a "1.5-cm cathode" [27]. The data used in this study was obtained as part of long-duration (~2000 h) wear testing in two nearly identical discharge setups at JPL facilities [28]. In the first test the cathode was operated for 2000 h with propulsion grade (99.995% pure) Xe. The second test was operated for 1800 h, at identical discharge conditions as the first, using propulsion grade Xe with 10 ppm of oxygen to simulate a contaminated propellant feed system. Compared to a smaller version of this cathode, the 1.5-cm cathode employed a larger, more robust sheathed heater design, and is schematically drawn in Fig 1-left. A water-cooled cylindrical anode made of copper and a current-carrying solenoid were used during the two wear tests as shown in Fig 1-right. The solenoid was designed to produce a largely axial magnetic field near the cathode centerline with magnitude that was approximately equal to that in HERMeS along the thruster centerline. Also shown in Fig 1-right is the LaB_6 cathode located to the left of the solenoid. Though not visible in Fig 1, it is noted that the plane of the keeper exit was approximately at the same axial location as the plane of the upstream entrance (facing the cathode) to the solenoid.

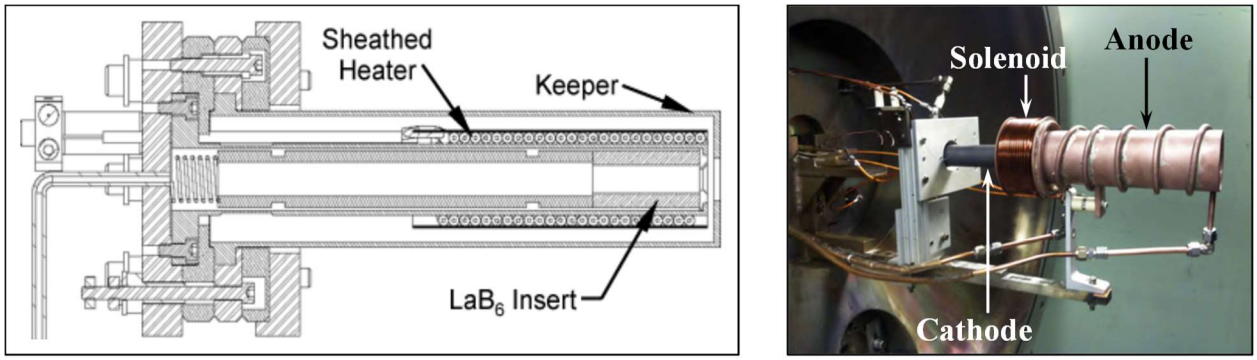

Fig 1. Left: Drawing of the LaB_6 hollow cathode used in the ~2000-h TDU wear tests. Right: Wear test configuration showing the water-cooled copper anode, solenoid, hollow cathode and mounting assembly on the right. (From Goebel, et al. [27])

In both the TDU-1 and TDU-2 tests, the discharge current of 25 A was regulated to simulate the nominal value in HERMeS (22 A), with an additional ~20% to account for current oscillations. Approximately every 500 h during the wear tests, cathode characterization measurements were performed to assess the performance of the device. As it will be explained in more detail later in this article, the discharge and keeper voltage are required as input to the OrCa2D simulations. To this end we have used measurements of the discharge and keeper voltages, taken at ~25 A and various xenon flow rates. The measurements from

the experiments will be labeled "Exp" throughout this article. The measured discharge voltage (V_d) from the cathode characterization tests is plotted in Fig 2-left. For convenience we have produced a best fit to these measurements shown as the dashed curve in Fig 2-left, and have used *it* to provide the required values at each flow rate in the simulations. For the keeper voltage only the values from the TDU 1 characterization tests were available. These values were averaged as plotted in Fig 2-right and, unless otherwise noted, they were used directly in the simulations as outlined in Sec. IV. A linear fit to the data also is plotted in Fig 2-right. The fit however will be used only in a single simulation at one flow rate to assess the sensitivity of the results, as it will described in more detail later in this article. In all other simulations the average keeper voltage measurements (symbols in Fig 2-right) were used. The peak-to-peak values of the keeper voltage oscillations, denoted as $V_{k\text{-}pp}$ in this article, were also monitored in the cathode characterization tests as part of the plume mode margin assessments. These measurements will be presented in Sec. IV and compared with simulations results.

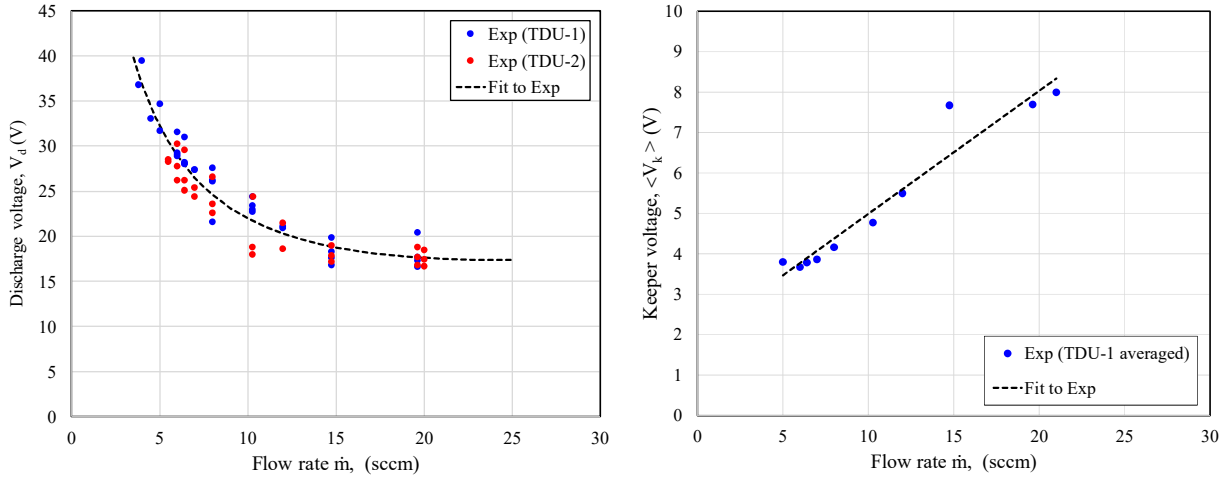

Fig 2. Measurements (labeled as "Exp") from the TDU-1 and TDU-2 ~2000-h wear tests of the 1.5-cm LaB_6 hollow cathode at JPL. Left: Discharge voltage as a function of xenon flow rate measured at different cathode characterization segments during each wear test [27]. Also plotted is a best fit to the measurements that will serve as input to the OrCa2D simulations. Right: (DC) Keeper voltage ($<V_k>$) as a function of flow rate. The symbols represent average values over the various cathode characterization segments during TDU-1.

III. Physics Models and Computational Methods

All simulations presented herein have been performed with the 2-D axisymmetric solver of the partially ionized gas in hollow cathode discharges OrCa2D. Development of the code began in 2004 and since then it has been used to simulate numerous different hollow cathodes and a wide range of operating conditions [19-22, 29, 30]. Comparisons with several plasma measurements (e.g. [10, 28]) has helped improve both our understanding of driving processes inside these devices as well as the fidelity of OrCa2D. In this section we provide some background about the code focusing on aspects that are most relevant to this work.

The physics models, conservation equations and numerical methods in OrCa2D have been described in detail in previous articles [19-22] and will only be described briefly here. The code solves the conservation laws for three species in the partially-ionized gas: electrons, xenon ions and xenon neutrals. It is assumed that only singly-charged ions are present and that quasi-neutrality prevails except inside sheaths which are handled with appropriate boundary conditions. The neutral gas inside these devices typically undergoes a transition from low-Knudsen-number, viscous, incompressible flow in the majority of the cathode interior to compressible flow and then to high-Knudsen-number flow in the keeper orifice and plume regions. Therefore the Navier-Stokes equations are solved for the neutral (xenon) gas only inside the cathode using an implicit backward Euler scheme. The transition to high Knudsen numbers is handled by specifying *apriory* a "transition boundary" at which the method to obtain the solution changes from the Navier-Stokes

equations to a collision-less approach that assumes neutrals follow straight-line trajectories [31]. The scheme ensures that mass and momentum are conserved across the transition boundary, and that at the transition boundary a smooth change of the mass flux across it is established. Most plasma equations are solved using strongly-implicit methods. The Euler equations for mass and momentum of ions are solved in the entire computational domain. A separate energy equation also is solved for the ions allowing for thermal non-equilibrium in the heavy species. Ionization, charge exchange and electron-ion collisions are accounted for in the equations and modeled as source or drag terms.

The electron properties are determined from the solution to Ohm's law and the energy and current conservation equations. When a magnetic field is applied the electron equations are discretized and solved on a magnetic-field-aligned mesh in regions where the Hall parameter exceeds unity [21, 32]. The largely collisional plasma in the interior of most electric propulsion hollow cathodes allows for a continuum description of the conservation laws, as confirmed by several results of OrCa2D simulations and plasma measurements [19-22]. The near-plume region of these devices however is more challenging. The first efforts to model the plume with OrCa2D revealed that the electron resistivity due to classical collisions can be orders of magnitude too low to explain the measured plasma parameters. Mikellides, *et al*. [17] postulated that the presence of anomalous resistivity in the plume of a hollow cathode was required to explain the rise of the plasma potential and electron temperature measured downstream of the orifice of a cathode operating at 25 A. It was also pointed out in [19] that the conditions for growth of IAT [33-35] existed downstream of the orifice exit, and that when an idealized anomalous resistivity model for the electrons subjected to IAT was included, the agreement with the measurements near the orifice improved significantly. The idealized IAT model of the resistivity was based on the formulations of Sagdeev and Galeev (S&G) [35] who assumed the IAT saturates through non-linear wave-particle interactions, enabling them to reduce the "anomalous" collision frequency ν_α to a simple algebraic function of the macroscopic plasma parameters, as follows:

$$\nu_\alpha = \alpha \omega_{pi} \frac{u_e}{C_s} \tag{1}$$

where the ratio of the electron to ion temperature (T_e/T_i) in the original formulation has been assumed here to be constant, and has been included in the coefficient α. This coefficient is determined in OrCa2D by iteration based on the specified discharge current. The electron drift speed is u_e, the ion acoustic speed is $C_s=(kT_e/m_i)^{1/2}$ and the ion plasma frequency is ω_{pi}. In OrCa2D, ν_α is added to the total resistivity η:

$$\eta = \frac{m_e}{q_e^2 n_e} (\nu_{ei} + \nu_{en} + \nu_\alpha) \tag{2}$$

where ν_{ei} and ν_{en} are the (classical) electron-ion and electron-neutral collision frequencies, respectively. This formulation for the anomalous frequency in OrCa2D led to simulation results that agreed well with experimentally-measured plasma parameters along the centerlines of two (BaO) discharge cathodes [17, 21] operating with discharge currents in the range of 13.3-27.5 A. The presence of IAT in the near-plume of hollow cathodes was later confirmed experimentally for the first time in a high-current (100 A) LaB_6 cathode as reported by Jorns, *et al*. [13]. Though the S&G wave-saturation model (Eqs (1) & (2)) appeared to capture well the IAT-driven anomalous transport in low-current cathodes, more recent work with OrCa2D has suggested that the assumptions which led to the S&G scaling of the anomalous collision frequency failed at higher discharge currents. Thus, a model of the IAT derived directly from kinetic theory has been incorporated in the code by Lopez Ortega, *et al*. [32] that treats waves as quasi-particles. The kinetic-based model allows for more accurate simulations of high-current cathodes but requires the solution

of an additional conservation equation for the turbulent wave energy. Since the cathode we are investigating here operates nominally at a discharge current of <25 A, we have assumed IAT saturation and used Eq. (1) to determine the anomalous collision frequency. It is possible that this choice may prohibit us from capturing any coupling that may be occurring between ionization modes (if they are present) and the IAT at the intermediate frequencies (~50-500 kHz) since the S&G model does not account for the growth of the acoustic waves to the saturated state. Therefore, if the S&G model reveals that ionization modes are present and captured by the OrCa2D simulations, we plan to invoke in the future the kinetic-based model by Lopez Ortega, *et al*. [32].

The emitted electron current density from the insert is specified according to the Richardson-Dushman equation for thermionic emission [36]. Recently, OrCa2D has been coupled with a 2-D axisymmetric thermal model of the cathode that yields the emitter temperature self-consistently. A description of this new capability is reported in our companion paper by Guerrero, *et al*. [37]. When OrCa2D is not coupled to the thermal model the emitter temperature is specified using a 4^{th}-order polynomial. A more detailed description of how the emitter temperature is used in the spot-to-plume mode investigations is provided in later sections. The field-enhanced emission due to the Schottky effect is included as derived in [19], and its implementation in OrCa2D is provided in [38]. The value of the work function is taken to be 2.67 V from [39] and is based on measurements of the zero-field saturated current density obtained at various temperatures. An experimental and numerical investigation with a similar LaB_6 cathode by Guerrero, *et al*. [37] has shown that this value of the work function may in fact be lower, which would imply lower temperature for a given emission current density. Since it is the emission current that is of most significance on mode transitions we argue that the precise combination of emitter temperature and work function is of no major significance to this investigation and therefore have retained the value of 2.67 V. It is important to emphasize that net emission is determined not only by the emission current density but also by the current density of electrons that are absorbed by the emitter wall. This is also account for in OrCa2D as described in [19, 20]. For boundaries that are electrically conducting electron and ion collection is captured in the code in both ion-attracting and an ion-repelling sheaths. This boundary condition was described in detail in [30]. At the anode, current is collected based on a specification of the measured discharge current. Ions that strike the anode are assumed to get neutralized and return back to the computational region as neutrals with a thermal speed that is based on the specified temperature of the anode.

In the experiments a cylindrical anode was used that was in close proximity to the cathode. The computational domain in the vicinity of the cathode plate and near plume is outlined in Fig 3. The full domain from a representative simulation of the TDU LaB_6 cathode is shown in Fig 4. The two figures provide also naming conventions for the various cathode components and boundary conditions cited throughout this article. L_{em} denotes the length of the emitter. The length of the interior cathode region, defined from the inlet boundary at z=0 to the entrance of the first orifice is designated as L_{in}. Also shown in Fig 3 is the location of the solenoid used in the experiments (Sec. II) to apply the magnetic field. The solenoid is only schematically depicted in Fig 3, so its true length and number of coils are not as shown in the figure. In the experiments the diameter of its inner coil was approximately equal to the outer diameter of the cylindrical anode and the plane of its upstream entrance was at the same axial location as the plane of the anode's upstream entrance. Both planes were also at the same axial location as that of the keeper electrode facing the cathode plume. The (2-D axisymmetric) solenoid magnetic field has been closely replicated in the simulations. the wear and characterization tests the keeper collected zero net current (floating). All these specifications have been incorporated in the simulations. Regarding the floating keeper, in OrCa2D we iterate on the keeper voltage until this condition is met. A zero-current condition also is specified at the outflowing boundaries (Fig 4). It is worth noting that in the present simulations we found that current collection at the inner surfaces of the keeper was not negligible. Thus, we extended the computational domain to include a region along the inner surface of the keeper tube, as shown in Figs 3 & 4.

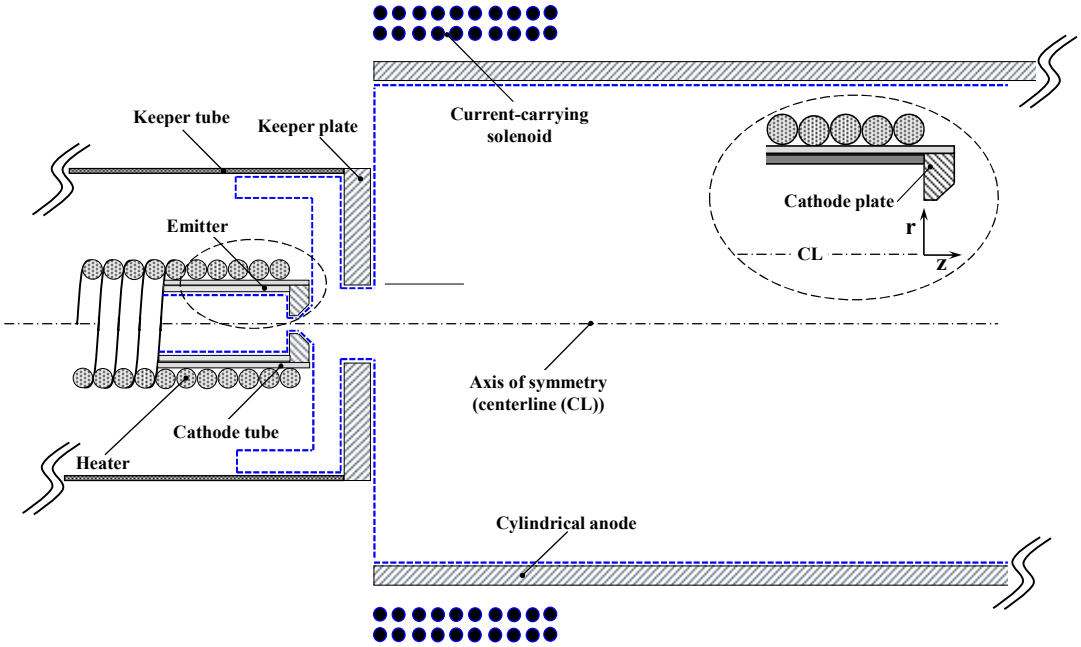

Fig 3. Schematic of the computational domain (blue dashed outline) used in the OrCa2D simulations, in a region near the cathode electrodes and plume (not to-scale).

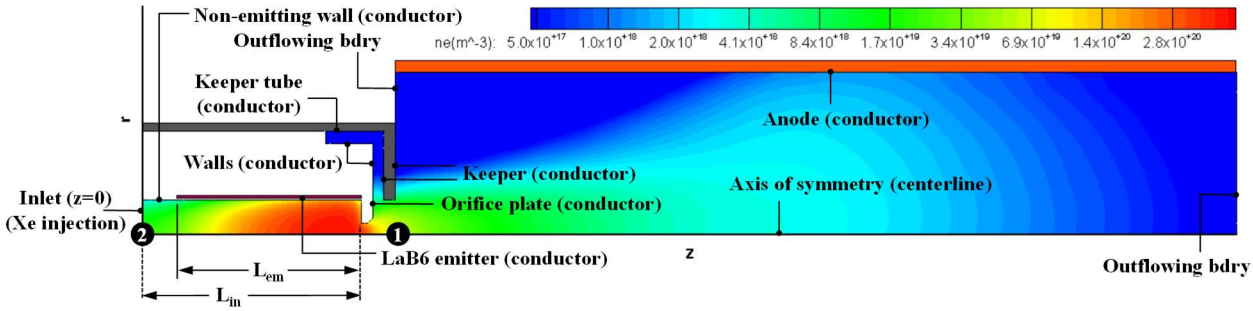

Fig 4. Numerical simulation domain (to-scale) showing a representative OrCa2D solution of the electron number density in the LaB_6 cathode. Also shown are the locations of two numerical probes (numbered 1 and 2) used to monitor the solution and naming conventions for boundaries and length scales, as used throughout this article. The solenoid is not shown.

IV. Spot-to-plume Mode Investigations: Numerical Simulations and Comparisons with Measurements

Probe measurements have shown that when the discharge is in plume mode the plasma is relatively quiescent in the cathode interior [10]. This suggests that the transition from spot mode is initiated by process(es) in the plume of the cathode. Nevertheless, since plume mode is typically reached as $I_d/\dot{m}$ increases, a natural question is: how does the plasma evolve inside the cathode as this ratio changes? More specifically, as the flow rate is reduced (at fixed current) for example, are the plasma fluxes to the emitter sufficient to sustain high enough temperatures for emission? If yes, how are they sustained since, naturally, a lower number of neutrals is supplied to the cathode at the lower flow rates? It is very difficult to obtain a detailed picture of how the emitter temperature evolves with the plasma in two dimensions without coupling the plasma solver with a thermal model of the cathode. For this reason work has begun at JPL to pair OrCa2D with a thermal model of the cathode. A thermal model of same LaB_6 cathode that is being investigated here but with an emitter that is smaller by 50% in the inner diameter has in fact already been

developed in the COMSOL Multi-physics® heat transfer module, and validated by experiments. The numerical strategy followed to link it to OrCa2D and results from the first coupled plasma-thermal simulations are reported by Guerrero, *et al*. [37] in our companion paper. While the maturity and fidelity of this new capability is advanced, we argue that some insight can already be gained from existing measurements to begin answering the abovementioned questions.

Though no emitter temperature measurements are available in the LaB_6 cathode studied here, the measurements taken in the same cathode with the smaller emitter (used in Guerrero, *et al*. [37]) reveal only small temperature changes with flow rate. These measurements are plotted in Fig 5-left, where the normalized temperature T'_{em} is defined as the ratio of $T_{em}/T_{em\text{-}max}$, with $T_{em\text{-}max}$ being the maximum value measured along the emitter after considering all the flow rates. The temperature plots in Fig 5-left are 2nd-order polynomial fits to measurements from three thermocouples placed equidistantly from each other along the emitter [37], and are plotted as a function of x/L_e. Here x is the distance from the tip of the emitter that is furthest away from the orifice. For all flow rates plotted in Fig 5-left the discharge current was 25 A. The comparison between flow rates ranging 5-25 sccm show a maximum difference in the emitter temperature of less than 46 ºC (<4% of the max), which is less than the maximum difference along the emitter for any given flow rate. Similarly small changes in temperature with flow rate were found by Polk, *et al*. [41] in an NSTAR-like (BaO) discharge cathode: at a discharge current of 12 A the maximum temperature change was less than 20 ºC (<2% of the maximum) in the flow rate range of 5.5-10 sccm. More interestingly however, we see in Fig 5-left that the temperature in general increases with decreasing flow rate, leaving unsupported the hypothesis that plume mode may be driven by excessive cooling of the emitter due to reduced plasma heating. The same trend was observed in the NSTAR-like cathode by Polk, *et al*. [41].

It is well understood that the characteristic times associated with the thermal response of the cathode system are much longer than those associated with changes in the plasma. The latter includes of course the dynamics associated with the keeper voltage oscillations we are seeking to study here. Furthermore, the observed trends of the emitter temperature with flow rate, combined with the results by Goebel, *et al*. [10] regarding the dynamically benign response of the interior plasma for a wide range flow rates, suggest that the discharge adjusts itself to provide the necessary fluxes for self-heating operation. As it will be shown later in the paper, this self-control with decreasing flow rate is achieved mainly by a rise of the plasma potential and electron temperature inside the cathode. All in all, these facts suggest that it may still be possible to investigate the driving physics behind spot-to-plume mode transition without a coupled plasma-thermal simulation. Indeed, we have followed this approach here as we explain below.

The numerical simulations have been conducted as follows. The mass flow rate and discharge current are required as inputs to OrCa2D. They are therefore specified directly in the code. We have performed simulations at 5, 6, 8, 10, 14.8 and 20 sccm while keeping the discharge current fixed at 25 A. To achieve this value of the current an iteration is performed on the anomalous transport coefficient α in Eq. (1). The discharge voltage also is specified in the simulations using the fit to the measurements in Fig 2-left. The TDU cathodes had an emitter with an inner diameter that is 50% larger than that investigated by Guerrero, *et al*. [37], for which temperate measurements exist (see Fig 5-left). Most of the other measurements that are relevant to our investigation however were made in the TDU cathodes, not the one studied by Guerrero, *et al*. [37]. Moreover, the TDU cathodes were operated with an applied magnetic field whereas the smaller cathode was not. Attempts to obtain emitter temperature measurements in the TDU cathodes yielded ambiguous results. Thus, in our simulations we assume a spatial variation of the temperature along the emitter that is based on insight gained from previous OrCa2D simulations and comparisons with plasma measurements in this same cathode. The variation we have assumed is plotted in Fig 5-right, where the normalized temperature T'_{em} is as defined previously (Fig 5-left). We note that a drop in the temperature of about 25% (almost 400 ºC) is applied in this TDU cathode (Fig 5-right), which is larger than that measured in the cathode with the smaller emitter (Fig 5-left). This is mainly due to the large plasma density drop that is observed in this cathode with distance from the orifice (to be presented in a later section), leading to reduced heating of the upstream portions of the emitter. Though the axial variation along the emitter (Fig 5-right) is kept unchanged for all flow rates the temperature is allowed to change during a simulation. The process is described in more detail in the next section.

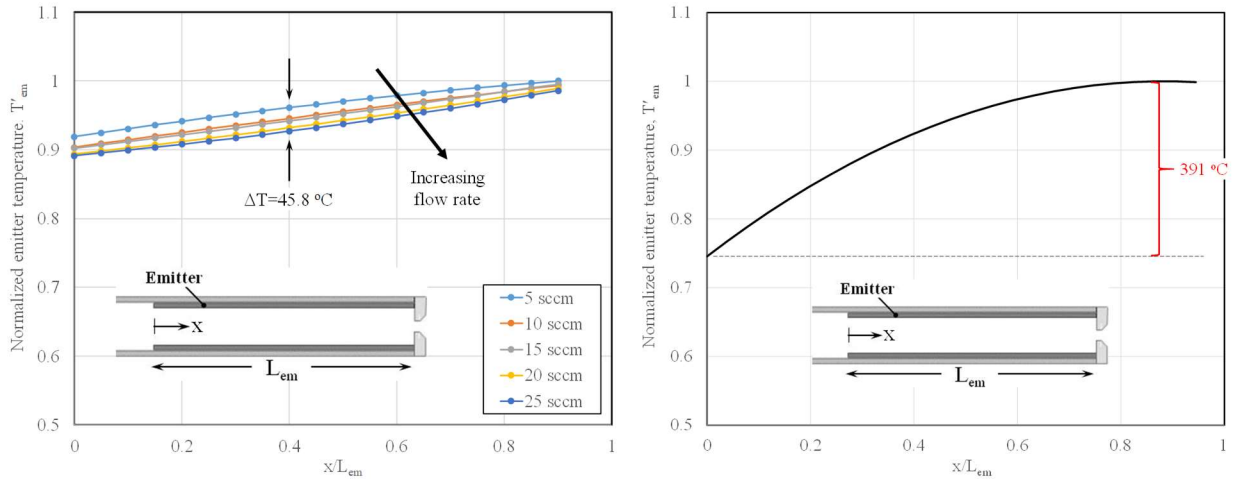

Fig 5. Left: Polynomial fits to measurements obtained by Guerrero, et al. [37] from three thermocouples placed in a LaB_6 cathode operating at 25 A. The cathode had the same dimensions as the one studied here but the insert had a 50% smaller inner diameter and an 8.5% smaller length. Also, the cathode was operated without an applied magnetic field. Right: Temperature variation along the LaB_6 emitter used in the OrCa2D simulations of the mode dynamics. The distance from the end of the emitter furthest away from the orifice is x.

A. **Model validation: Comparisons between simulations and plasma measurements at the nominal flow rate for HERMeS**

At its nominal operating condition of 14.8 sccm and 25 A, the TDU cathode is in the so-called spot mode during which the plasma plume is visibly quiescent and the peak-to-peak oscillations of the keeper voltage, $V_{k,pp}$, are less than 7% of the $<V_k>$. Prior to the TDU wear tests, plasma measurements using injected probes along the centerline of this cathode provided the electron number density, plasma potential and electron temperature as plotted in Fig 6. Though these measurements were made at a slightly lower flow rate (13.1 sccm), we use them here to compare with the OrCa2D simulations performed at the nominal value (14.8 sccm). The maximum emitter temperature $T_{em\text{-}max}$ was determined by iteration during the simulation, until the desired (DC) keeper voltage was achieved. This value of $<V_k>$=7.68 V was specified based on the TDU-1 wear test measurements in Fig 2-right. With the variation of the temperature along the emitter specified as in Fig 5-right, $T_{em\text{-}max}$ is all that is necessary to obtain the entire T_{em} as a function of x/L_e.

The chamber backpressure (p_B) was measured about 1 m away from the cathode and monitored throughout the duration of the TDU wear tests [27]. An average value of 0.35 mTorr (3.5×10^{-4} Torr) was specified in the simulations based on the overall history of the backpressure from both wear tests. Since the measurement was far from the test assembly it is recognized that this value could have been higher near the cathode. This is an important observation as it will be discussed later in this article. It is also noted that inside the cylindrical anode the gas pressure is expected to be higher than the measured backpressure under nominal operating conditions, due to the xenon flow from the cathode and the return (back to the plume) of plasma ions as atoms after striking the anode. All these effects are already accounted for in the simulations.

The comparisons between the simulation results and injected-probe measurements along the cathode centerline are depicted in Fig 6. Though the simulation is within the experimental uncertainty of the plasma density measurement in Fig 6-left, there appears to be a trend in the discrepancy between them that places the simulation result more forward axially than the measurement. Also, in general, the density is lower in magnitude inside the cathode but higher outside. Since it is known that the interior plasma contracts and moves forward with increasing flow rate [e.g. see [43]], some part of this discrepancy trend is associated with the 13% higher flow rate specified in the simulation. Though not yet quantified, the effects of the probe injection on the measurement also could have played a role here, similarly to the known effects of probe perturbations in Hall thruster discharges [44]. Also lower but within the experimental uncertainty are the simulation results for the electron temperature as shown in Fig 6-right. Regarding the plasma potential,

the three available measured values seem to suggest a small increase with distance from the orifice, towards the interior of the cathode. This is in contrast to the simulation result which shows a clear decrease. This discrepancy trend was observed and discussed in the past in a different cathode [45], and more recently in the same cathode that is being simulated here [42]. Briefly, we have argued that the data do not follow the result predicted by Ohm's law even when the measured electron temperature and density are used directly to determine the value of the potential. Considering the short mean free paths of the plasma in this region of the cathode, we have no reason to believe that Ohm's law is violated here. Hence we have argued that the plasma potential measurements must carry a larger uncertainty than the error bars in Fig 6-right indicate.

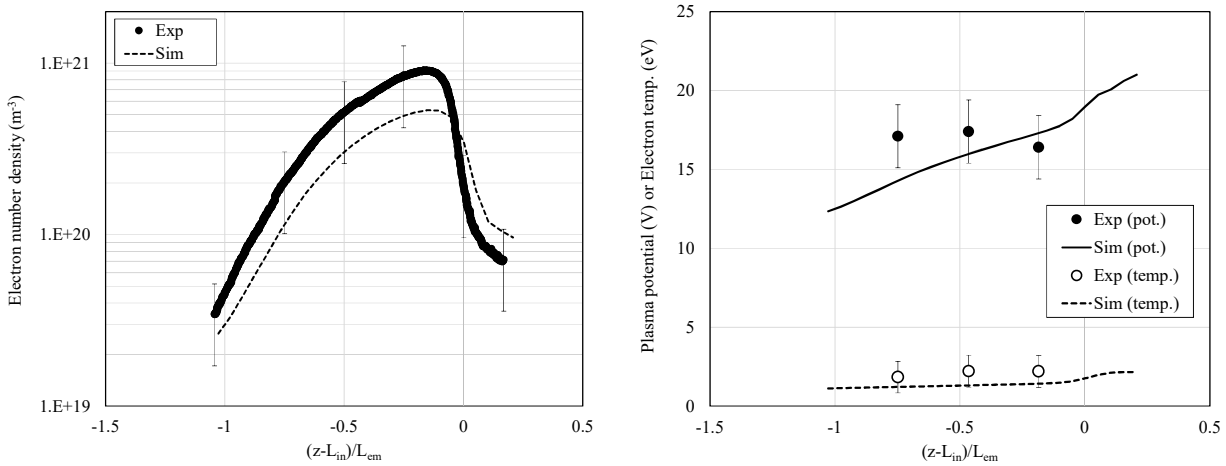

Fig 6. Comparison of the steady-state solution from the OrCa2D simulations (denoted as "Sim") with measurements along the centerline of the TDU (LaB_6) cathode when operated in spot mode and a discharge current of 25 A. The measurements were taken prior to the TDU wear tests, when the flow rate was 13.1 sccm. The simulations specified the wear-test values of flow rate (14.8 sccm) and backpressure (0.35 mTorr). Referring to Figs 3 & 4, the location of the entrance to the cathode plate orifice is at $(z-L_{in})/L_{em}=0$

B. **Simulation results at different flow rates and fixed backpressure**

As part of the characterization tests the xenon flow in the TDU cathodes was varied to determine the so-called plume mode margin. This is typically determined by measuring changes in $V_{k,pp}$ as a function of flow rate and discharge current. In this section we perform simulations at flow rates ranging 5-20 sccm, each at fixed discharge current of 25 A. The objective is to investigate the behavior of the solution at each condition, focusing on possible plasma dynamics that may explain the observed rise of the keeper voltage fluctuations as the flow rate is reduced, that is, as the cathode transitions from spot to plume mode. As in the simulation at 14.8 sccm (Sec. IV.A), the discharge voltage at each flow rate is specified based on the fit to the measurements shown in Fig 2-left. Also, as in the previous simulation, the emitter temperature is determined by iterating on $T_{em\text{-}max}$ until the simulation reaches a value of $<V_k>$ that is close to that measured value in the TDU-1 characterization tests (Fig 2-right).

The backpressure in this series of simulations was deliberately held fixed at the value of 0.35 mTorr for all flow rates, for reasons that will become clear in the next section. During each simulation the evolution of the solution was monitored by several numerical probes positioned throughout the computational domain. A convergence criterion was implemented in OrCa2D that is based on the time-averaged computed variables to allow for a more consistent definition of a "steady-state" solution. The algorithm computes the % change in the main plasma variables within a specified time increment, from all numerical probes, and terminates the simulation when the maximum % change is less than a specified value. In the present simulations the convergence criterion was set to 0.002% for all flow rates.

The steady-state results for the keeper voltage and maximum emitter temperature are shown in Fig 7-left. The temperature has been normalized to the maximum value obtained after the simulations at all flow rates reached a steady state. The emitter temperature changes are found to be very small, <0.5%, in the

range of flow rates we have simulated (5-20 sccm). The explanation for this lack of sensitivity on the xenon flow rate is as follows. As the flow rate decreases at fixed discharge current, the discharge voltage increases (Fig 2-left). This is accompanied by an increase of the plasma potential. This increase of the potential was expected but it was not clear, prior to the simulations, if such increase would have occurred mostly in the plume region of the cathode, through a rise of the resistivity there, or whether it would be more global. The simulations reveal both a global increase of the potential but also a rise of the electric field in the plume region, as shown in Fig 7-right. For example, from the orifice entrance, $(z\text{-}L_{in})/L_{em}=0$, to the location in the plume where the maximum potential is reached, the difference is ~9 V and ~17 V at 14.8 sccm and 5 sccm, respectively. The higher electric field leads also to higher electron heating in the cathode plume as suggested by the elevated electron temperatures in Fig 7-right.

As the flow rate is reduced the major consequence of the higher potential and electron temperature in the cathode interior is the regulation of the sheath drop along the emitter, which controls the particle and energy fluxes back to it. The discharge current then is found to be regulated by the plasma itself, not by the thermionic emission of electrons through changes in the emitter temperature. This is likely due to the much longer characteristic times that are required by the cathode system to respond thermally to changes in the operating conditions than the plasma itself. A final noteworthy finding associated with the steady-state solution is that the measured keeper voltage could not be achieved by the simulations as the flow rate was reduced below ~10 sccm, unless the computational domain was extended to include the region shown in Fig 4 along the interior of the keeper tube. This is because the plasma does indeed extend to these interior regions of the cathode as the flow rate decreases thereby contributing to the total current collected by the keeper. When this region was excluded, a larger $\langle V_k \rangle$ than the measured value was required to float the keeper at the lower flow rates.

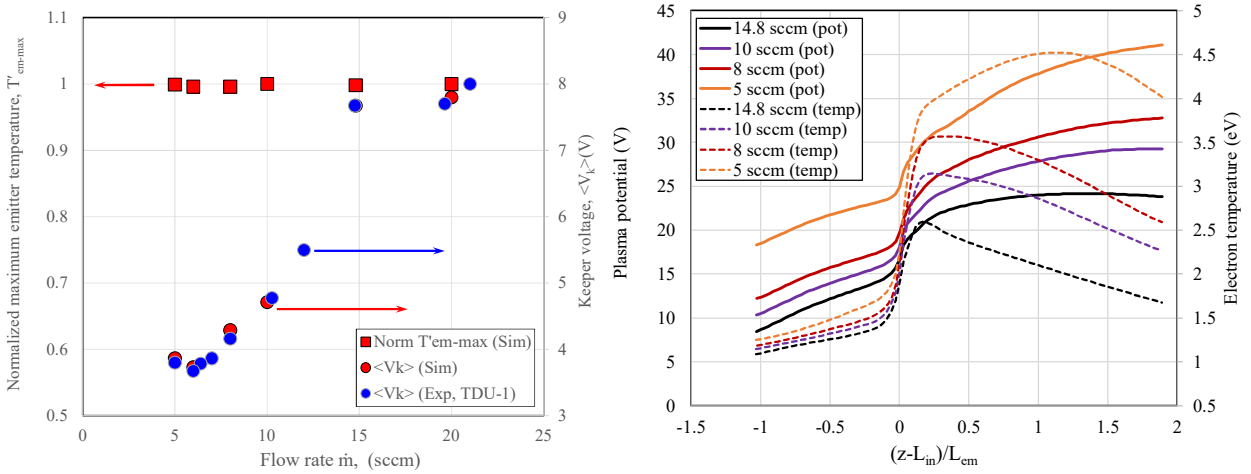

Fig 7. Steady-state results from OrCa2D simulations with fixed backpressure (0.35 mTorr). Left: Keeper voltage and maximum emitter temperature. The latter has been normalized to the maximum value found after all the flow rates reached a steady state, $T'_{em\text{-}max}$. The computed $\langle V_k \rangle$ is compared to measurements obtained during the TDU-1 wear test (also in Fig 2-right). Right: Computed plasma potential and electron temperature along the cathode centerline at different flow rates.

The history of the computed keeper voltage at different cathode flow rates is plotted in Fig 8-left. The plotted result for each flow rate started from a previous OrCa2D solution that was arbitrarily close to the steady-state value. Thus, no special attention should be given to the long time scales and the specific manner in which the solution reaches a steady state. Rather, the result of significance is associated with the short time scales. Specifically, the results show small-amplitude oscillations that increase in magnitude as the flow rate is decreased. To assess the sensitivity of these oscillations on the keeper voltage the solution at 14.8 sccm using $\langle V_k \rangle$=6.25 V also was obtained, instead of the nominal 7.68 V, and is also plotted in Fig 8-left for comparison. This value was chosen based on the linear fit to the TDU-1 measurements plotted in Fig 2-right. A more clear illustration of the rise in the amplitude of the oscillations is shown in Fig 8-right

which compares the % change in the keeper voltage at 14.8 and 5 sccm relative to a time-smoothed solution obtained using an adaptive data-smoothing algorithm. The time-smoothed solution represents here the $<V_k>$ For this comparison we have used the 14.8-sccm solution at $<V_k>$=6.25 V for illustrative purposes as it exhibits larger-amplitude oscillations than those at $<V_k>$=7.68 V.

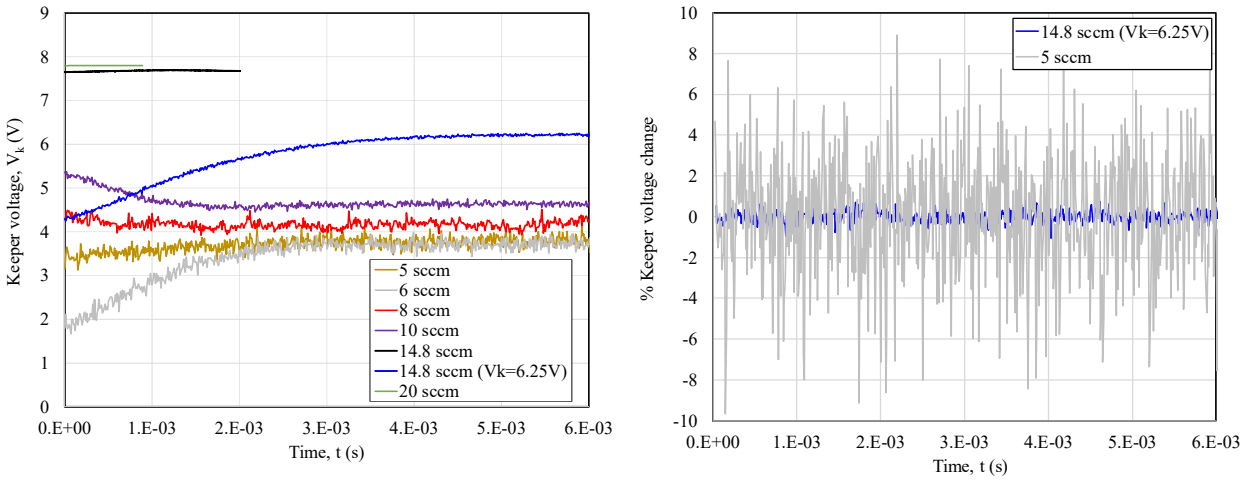

Fig 8. History of the keeper voltage at different flow rates from the OrCa2D simulations at fixed backpressure. The initial condition for each flow rate was set from a previous OrCa2D solution that was arbitrarily close to the steady-state value. Left: Keeper voltage as a function of time for the range 5-20 sccm. Right: %-change in the keeper voltage relative to $<V_k>$ (from Fig 2-right) for 14.8 and 5 sccm.

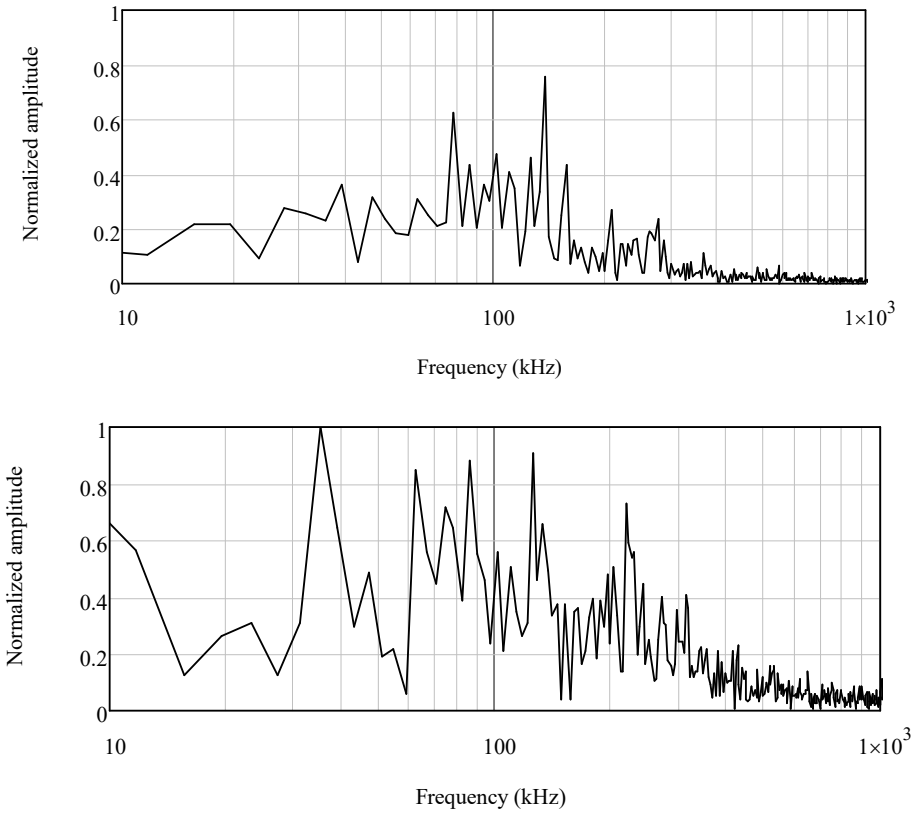

Fig 9. Fast Fourier transforms of the computed peak-to-peak oscillations in the keeper voltage ($V_{k\text{-}pp}$). Top: 14.8 sccm ($<V_k>$=6.25 V). Bottom: 5 sccm.

A closer examination of the oscillations reveals several noteworthy findings. First, fast Fourier transforms (FFT) of the time signals show relatively broad spectra with highest frequencies ranging between tens and a few hundred kHz. No particularly dominant frequency was detected. An example of the FFTs from the simulations at 14.8 sccm ($<V_k>$=6.25 V) and 5 sccm is shown in Fig 9. Second, these oscillations appear to be associated with a dynamically active region of the discharge in the vicinity of the keeper plate surface facing the plume, between the core plasma and the anode. As we move radially inward towards the bulk plasma in the plume, the oscillations are found to diminish. Also, negligible plasma oscillations are found in the cathode interior. The dynamically active region is loosely identified by the dashed circle in Fig 10. Here is where we find the steepest gradients of the electron number density due to the presence of the largely axial applied magnetic field. In fact, as the anode is approached the density is found to fall to the minimum value, which was set to be 10^{14} m^{-3} in all the simulations. Though an increase to 10^{15} m^{-3} was not found to affect the dynamical behavior of the plasma significantly, the proximity of the boundaries to this region, especially that associated with the outflowing condition (see Fig 4), raises the question of whether these oscillations are excited fully or partially by the numerical scheme. To assess this, we extended the keeper boundary condition all the way to the anode, effectively replacing completely the outflowing condition with a conducting wall. At 14.8 sccm no significant change in the dynamical behavior of the solution was found but no other flow rates were simulated with this BC.

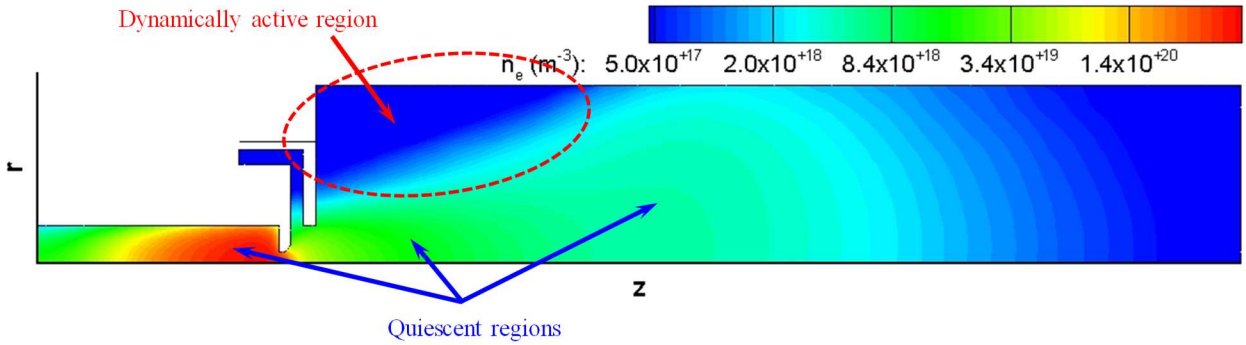

Fig 10. Time-averaged solution of the electron number density (n_e) at 8 sccm showing the region where plasma oscillations are most active. The simulation assumed the same backpressure as that for 14.8 sccm (namely 0.35 mTorr).

There is further evidence to suggest that the oscillations in this region are physically induced (rather than numerically). The computed peak-to-peak oscillations in the keeper voltage are plotted as a function of xenon flow rate in Fig 11-left. Also plotted in the same figure for comparison are the measured values obtained during the TDU cathode characterization tests. A best fit to the data also is shown to better illustrate the comparison with the simulations. It is evident from this comparison that the simulations predict much smaller values of $V_{k\text{-}pp}$ than the measurements. However, if the computed and measured oscillations are normalized relative to their respective values at high flow rates, the dependence of the relative change in $V_{k\text{-}pp}$ on the flow rate is found to be in close agreement. The normalized values are denoted $V'_{k\text{-}pp}$ and plotted in Fig 11-right.

The rise of $V_{k,pp}$ with decreasing flow rate is found to be driven by the abovementioned dynamically active region in the near anode plume where the plasma density diminishes rapidly. This implores a closer investigation into the behavior of the neutral and electron number densities in the entire cathode plume. The time-averaged steady-state contours from the simulations at 14.8 and 8 sccm are shown in Fig 12 left and right, respectively. The top row depicts contours of the neutral number density and the bottom shows the electron number density. The plasma plume at 8 sccm is found to be somewhat more contracted than that at 14.8 sccm with lower electron density throughout the region. No major differences are found in the cathode interior between the two flow rates. The most clear distinction however is observed in the neutral gas, with the 8 sccm case exhibiting significant depletion of the plume gas downstream of the keeper. A

plot of the computed number densities along the cathode centerline in Fig 13 shows that the plume neutral gas density at 8 sccm is at least ~5× lower than that at 14.8 sccm.

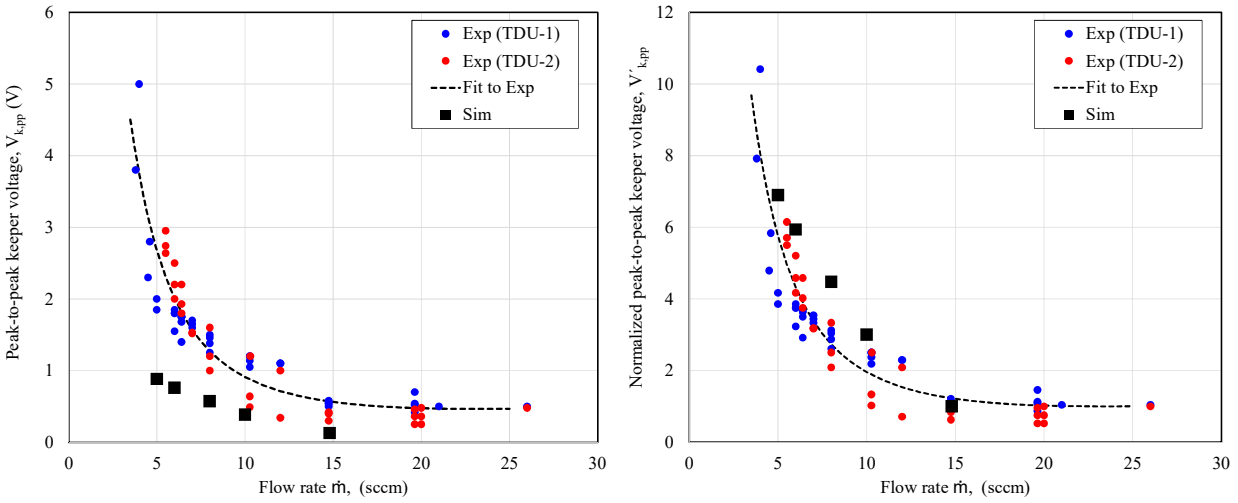

Fig 11. Comparisons between simulations and cathode characterization measurements of the peak-to-peak keeper voltage fluctuations (V_{k-pp}). Left: V_{k-pp} as a fucntion of Xe flow rate. Right: Normalized value, V'_{k-pp}, as a function of xenon flow rate. The simulation and experimental results were normlaized relative to V_{k-pp} at 14.8 sccm and 23 sccm, respectively.

Most importantly however, the 8-sccm solution shows that the neutral gas in this region has been depleted down to the density of the background neutrals set by the specified backpressure of 0.35 mTorr. This suggests that the sustainment of the discharge in the near-plume region of the cathode becomes more dependent on the background neutrals as the flow rate is reduced. This is because the cathode flow can no longer provide sufficient neutrals to support the ionization rates needed to sustain the discharge at the lower flow rates in this region. The ionization rate is higher here as the flow rate is reduced because the plasma potential and the electron temperature increase (Fig 7-right). Since at the low flow rates ionization in the depleted zone can be supported only by background neutrals, the density of which is held fixed for all flow rates in this series of simulations, it is precisely this increase in the temperature that drives the higher ionization rates in this region. For example, it is found that the maximum degree of ionization at 8 sccm is $n_i/(n_i+n_n)=0.7$ and occurs at $(z-L_{in})/L_{em}=0.36$, which is about 2× higher than the corresponding value at 14.8 sccm. (Note: since we only account for singly-charged ions and assume quasi-neutrality in the simulations the ion number density, n_i, equals n_e). The depletion of cathode neutrals then clearly requires a more careful examination of the background gas model in this region of the discharge, and is the topic of the next section.

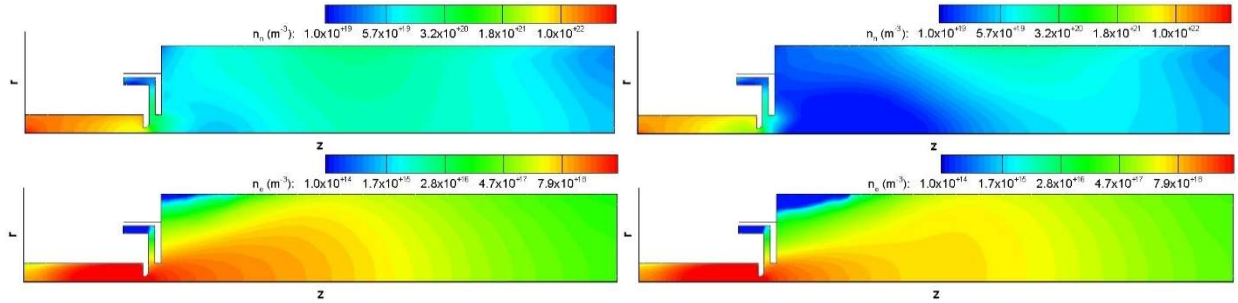

Fig 12. Time-averaged contours of the computed neutral (n_n, top row) and electron (n_e, bottom row) number densities from the OrCa2D simulations at 14.8 sccm (left column) and 8 sccm (right column). At 14.8 sccm, $<V_k>=6.25$ V. The backpressure was specified to be 0.35 mTorr in both cases.

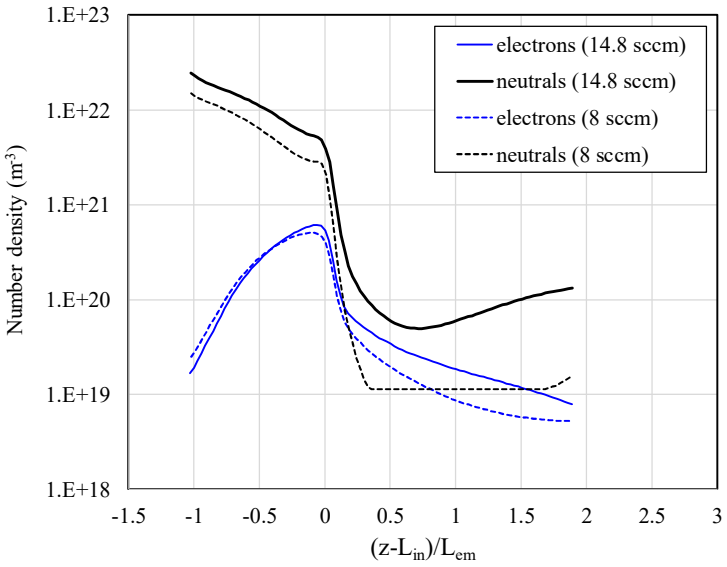

Fig 13. Computed neutral and electron number densities along the cathode centerline at 14.8 and 8 sccm. At 14.8 sccm, $<V_k>$=6.25 V. The backpressure was specified to be 0.35 mTorr in both cases. Noted is the region $0.3 \lesssim (z-L_{in})/L_{em} \lesssim 1.6$ in the plume where the neutral gas associated with the cathode flow has been fully depleted.

C. Effects of backpressure on the dynamics of the discharge

It is well known that the backpressure in the chamber is dependent upon the cathode operating flow rate. Without a global simulation of the gas flow in the facility and/or direct measurements it is not known precisely what this dependence is near the cathode. Therefore to obtain a preliminary assessment of the effects we assume here a linear dependence. In this linear model the average value measured during the TDU wear tests, 0.35 mTorr at 14.8 sccm, was used to scale the values at the other flow rates. The OrCa2D simulations from Sec. IV.B were then repeated. The only exception was that the backpressure varied according to the linear model plotted in Fig 14-left.

The simulations showed little to no differences when $\dot{m} \gtrsim 10$ sccm. However, a distinctively different dynamical response by the discharge was found when the flow rate was reduced to 8 sccm. We recall here that at 14.8 sccm (p_B=0.35 mTorr), the neutral gas density in the plume is still dominated by the cathode flow whereas at 8 sccm the cathode neutrals were completely depleted in a large region of the near plume (see Fig 12-top-right and Fig 13). The computed keeper voltage as a function of time for the varying-p_B simulations is plotted in Fig 14-right at four different flow rates. Compared to the results with fixed p_B (Sec. IV.B), it is found that the amplitude of the oscillations increases significantly when the flow rate is reduced to 8 sccm. A closer look at the 8-sccm signal (plotted again for convenience in Fig 15-left) reveals that the frequency spectrum is less broad than that plotted in Fig 9 (p_B=0.35 mTorr), exhibiting a most dominant frequency at about 5 kHz as illustrated by the FFT in Fig 15-right. The keeper voltage fluctuations are found to be driven by plasma oscillations in the near plume which exhibit the same dynamics. To illustrate this we also plot in Fig 15-left the plasma density as a function time at the keeper exit on the cathode centerline (location 1 in Fig 4). The interior plasma is found to be relatively quiescent as suggested by the low-amplitude oscillations computed near the cathode inlet (location 2 in Fig 4). This trace is also plotted in Fig 15-left. In a similar-size (BaO) cathode that was operated nominally with a 25-A discharge for a 20-50 kW ion engine, Goebel, *et al*. [10] measured what they termed "medium-frequency" plasma fluctuations, ranging 50-100 kHz. More specifically, when the cathode was operated at 4.5 sccm and without an applied magnetic field the plasma fluctuations were measured to be at a frequency of 80 kHz [10]. The authors found that this value was approximately equal to the ionization frequency of the plasma about 1 cm downstream of the cathode based on plasma measurements and an assumed fraction of ion to neutral densities (since the latter was not available from the measurements). Based on this they argued that these are ionization-driven oscillations. When the flow rate was increased to the nominal value of 5.5 sccm and

a (80-G) magnetic field was applied, the medium-frequency oscillations subsided to very small amplitudes. Finally, in agreement with our findings here, Goebel, *et al*. [10] found that the cathode interior was relatively quiescent. They measured only small-amplitude density fluctuations of the plasma inside this cathode when it was operated at 4.5 sccm and no magnetic field. These fluctuations were not correlated to the medium-frequency oscillations they measured in the plume.

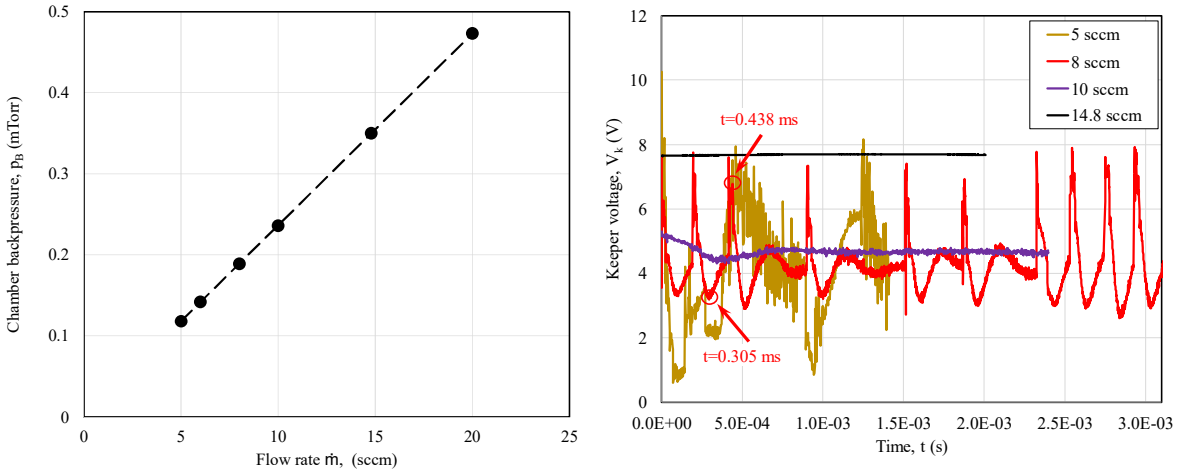

Fig 14. Left: Estimated backpressure during operation of the TDU hollow cathodes at different xenon flow rates. When the cathodes were operated at 14.8 sccm, the average value of the backpressure in the ~2000-h wear tests was approximately 0.35 mTorr, This value has been used here to scale (linearly) the backpressure at different flow rates. Right: History of the keeper voltage at different flow rates from the OrCa2D simulations. The backpressure at each flow rate was specified to values from the left plot.

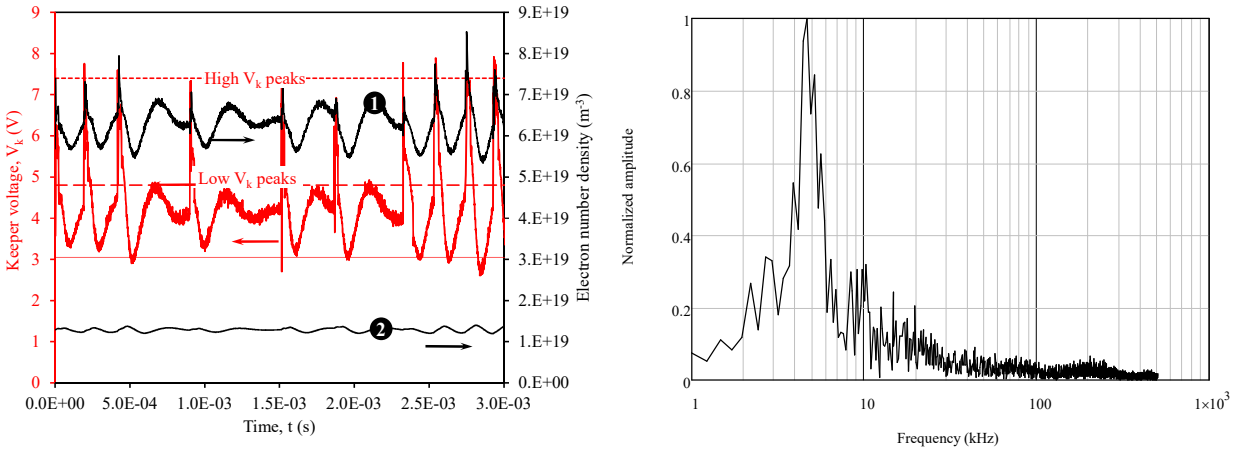

Fig 15. Simulation results at 8 sccm, with p_B=0.19 mTorr. Left: Oscillations in the keeper voltage showing spikes (high peaks) associated with attachment/detachment of the discharge to the anode and lower peaks associated with small axial contraction/expansion of the plume plasma. Also shown are traces of the electron number density at the keeper exit (location 1 in Fig 4) and cathode inlet (location 2 in Fig 4). Right: FFT of the time trace for V_k in the left plot. The dominant frequency is found to be 4.64 kHz.

Similarly to our findings here, Goebel, *et al*. [10] also found that their "medium-frequency ionization" oscillations occurred mostly in the near plume of the cathode whereas the interior exhibited negligible dynamic behavior. Moreover, regarding the nature of the oscillations, the solution for the TDU cathode at 8 sccm in Fig 15-left appears to exhibit a pattern that is very characteristic to an ionization oscillation. Indeed, we find that the ionization frequency in the region of the plume where the cathode neutrals have been depleted (see for example Fig 12-top-right) ranges 2-100 kHz, and that the frequency of the keeper

voltage oscillations is the same as the ionization frequency at about the center of the neutral-depleted region, $(z\text{-}L_{in})/L_{em}$=1.25. This is better illustrated in Fig 16 which plots the computed time-averaged ionization frequency along the cathode centerline at 8 sccm. Also plotted for comparison with Fig 13 are the neutral and electron number densities at both 14.8 and 8 sccm. It is noted that the minimum neutral gas density in plume at 8sccm is about 2× lower here than it was in the simulations with fixed p_B=0.35 mTorr. The dependence of the oscillations on the minimum neutral gas density and the correlation of the computed fluctuations in the keeper voltage with the ionization frequency both suggest that plume mode is indeed associated with neutral depletion and ionization-driven oscillations in the near-plume of the cathode. To further elucidate the dynamic behavior of the discharge during this mode we plot in Fig 17 the computed electron number density at two times, t=0.305 ms and 0.438 ms. These times are a representative pair of high and low peaks in the keeper voltage, as shown in Fig 14-right. It is observed that the motion of the plasma here is no longer driven by broad-spectrum low-amplitude fluctuations in the near anode region, as was the case in the fixed-p_B results of Sec. IV.B. To the contrary, the density oscillations are longitudinal and global, with the highest peaks in Fig 15-left associated with attachment/detachment of the discharge to the anode. The lower peaks are found to be due to an axial contraction/expansion of the plume plasma. Based on this axial motion, we can estimate a wavelength λ of the plasma density fluctuation and a wave velocity. At $(z\text{-}L_{in})/L_{em}$=1.25 we find that $\lambda\approx$3.2 mm and therefore the wave velocity is approximately $2\pi f\lambda\approx$100 m/s, using the computed frequency of $f\approx$5 kHz. This value is much smaller than the ion sound speed (C_s=1485 m/s), the ion speed (2645 m/s) and the ion thermal speed (867 m/s) at this location, but is only two times faster than the local neutral gas speed (50 m/s). The fluctuation therefore does not seem to be associated with the motion of ions and/or their sound waves.

The distinctive dual mode in the oscillations at 8 sccm (contraction/expansion and anode attachment/detachment) is found to coalesce more into one mode as the flow rate is reduced further to 5 sccm. Hence, it is possible that the dual mode is only prominent at those spot-to-plume transitional flow rates in which the ionization oscillations just begin to affect the attachment of the discharge to the anode. It is also possible that the numerical solution at these transitional flow rates is more sensitive to some of our assumptions, which is a topic that will be explored further in the near future.

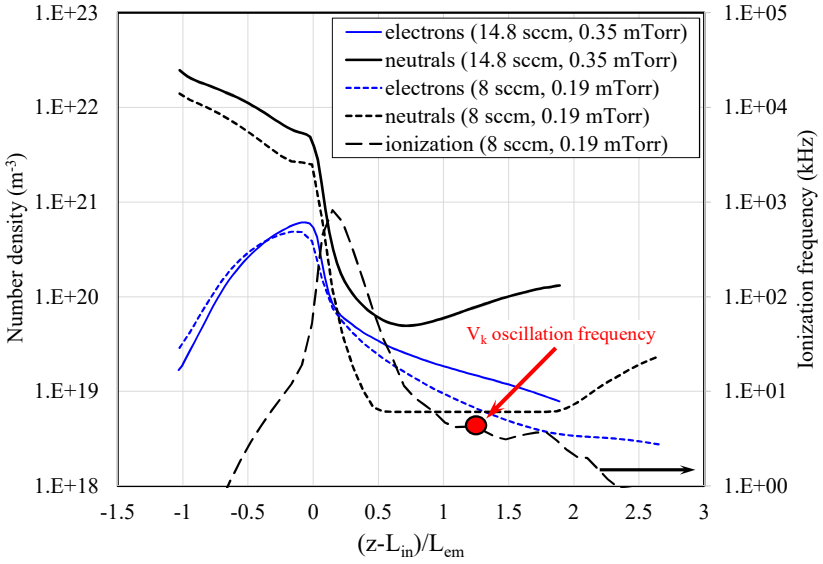

Fig 16. Computed neutral and electron number densities along the cathode centerline at 14.8 and 8 sccm (left axis) at different backpressures. At 14.8 sccm, $\langle V_k \rangle$=6.25 V. The plotted solution at 8 sccm is time-averaged. Also plotted is the ionization frequency (right axis) at 8 sccm and 0.19 mTorr. The value of the computed frequency associated with the keeper voltage oscillations equals the ionization frequency at about the middle of the region most depleted of neutral gas.

In Fig 18-left we plot a comparison of $V_{k\text{-}pp}$ between the simulations and the TDU cathode characterization tests. Unlike the comparisons of Fig 11-right, no normalization of $V_{k\text{-}pp}$ was employed here. It is found that the measured rise of $V_{k\text{-}pp}$ with decreasing flow rate is closely captured by the simulations. It is noted that for the 8-sccm solution we have included only the values associated with the low peaks in the keeper voltage (see Fig 15-left), since the high peaks are driven mostly by anode attachment/detachment events and are therefore more likely to be sensitive to numerical simulation assumptions than the low-peak motion. The average keeper voltage that each simulation ultimately reached after iteration on the emitter temperature also is compared with the measurements in Fig 18-right. As in the simulations with fixed p_B, no significant changes in the emitter temperature were found in the entire range of 5-20 sccm. The maximum temperature at the emitter was normalized to the highest time-averaged value obtained out of all flow rates we simulated, and is also plotted in Fig 18-right.

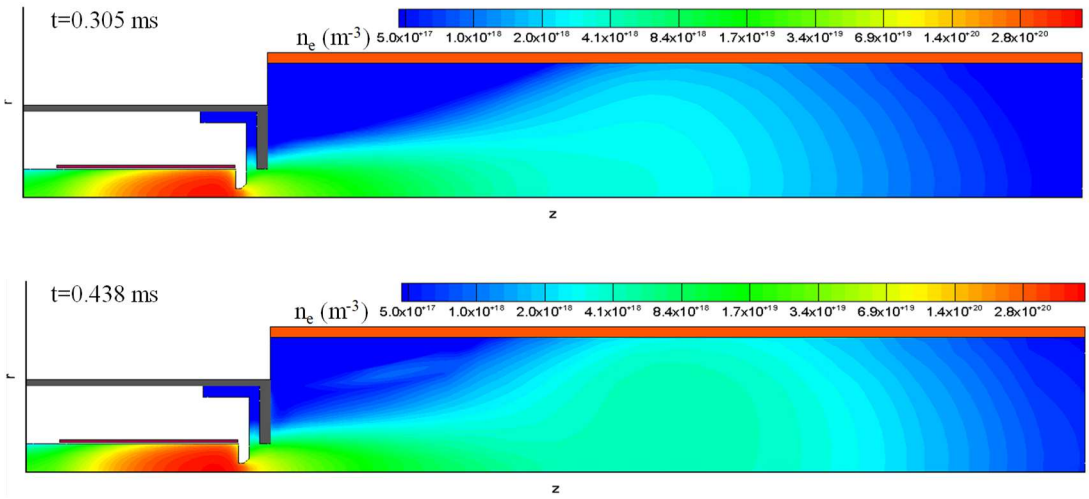

Fig 17. Contours of the electron number density (n_e) from the OrCa2D simulations at 8 sccm and p_B=0.19 mTorr, showing the spatial evolution of the plume at the lowest and highest value of the keeper voltage during one oscillation (see Fig 14-right).

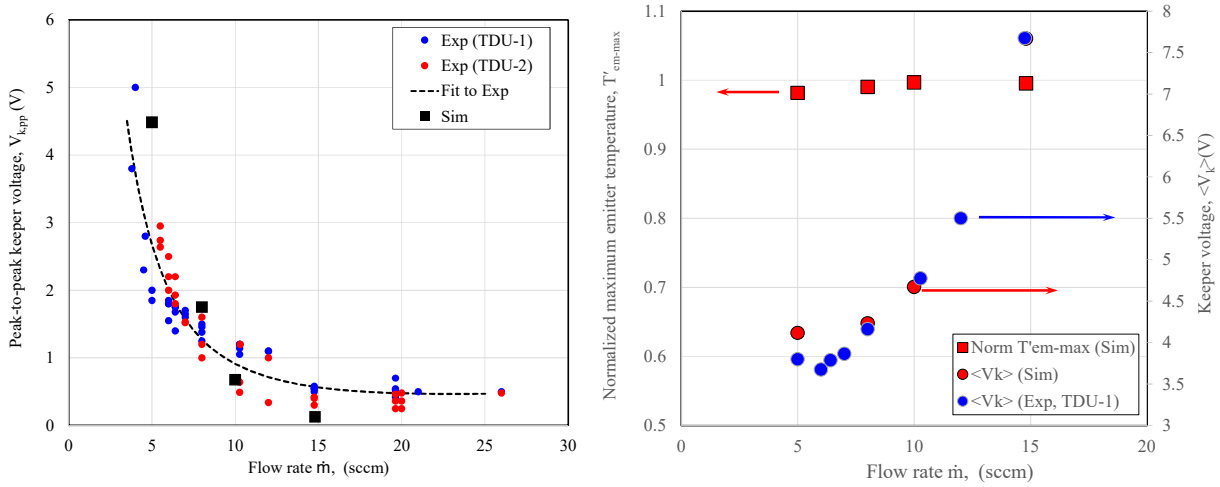

Fig 18. Left: Comparisons between simulations and cathode characterization measurements of the peak-to-peak keeper voltage fluctuations ($V_{k\text{-}pp}$) at different xenon flow rates. The simulations used a different backpressure at each flow rate based on a linear scaling from the wear test measurement at 14.8 sccm (see Fig 14-left). Right: Results from simulations of the keeper voltage and (normalized) maximum emitter temperature, $T'_{em\text{-}max}$. The computed <V_k> is compared to measurements obtained during the TDU-1 wear test. All values that are associated with oscillatory operating conditions have been time-averaged.

V. Conclusions

Ab initio models that allow for the prediction of the transition from spot to plume mode in hollow cathode discharges, across different geometries and operating conditions, have remained elusive since these modes were first observed in the laboratory over five decades ago. When in plume mode, experiments showed that a large luminous cathode plume develops where large-amplitude oscillations occur. In more recent investigations the measured power spectra in this region have confirmed the long-suspected presence of IAT, in the range of hundreds of kHz, but also revealed lower-frequency ($\lesssim$100 kHz) dispersion-less modes arguably associated with ionization instabilities. These low frequency modes became more dominant as $I_d/\dot{m}$ increased, that is, as the discharge was forced further into plume mode. The mode has also been observed in the laboratory to depend on the applied magnetic field and anode configuration.

These observations led to the conjecture that the transition from spot to plume mode is likely driven by ionization processes in the cathode plume. In Hall thruster cathodes nominally operate with flow rates that are higher than those in their ion engine counterparts for the same discharge current. Operation in plume mode is therefore less of a concern in Hall thrusters. Nevertheless if ionization in the plume are major drivers of the transition, a few questions arise. Specifically, how does the location of the cathode plume relative to the Hall thruster plume affect the transition? Is the plume margin from a stand-alone cathode test truly "similar" if a different anode arrangement is used than that in the thruster? What are the effects of facility backpressure on the transition? It is now also known that IAT in these discharges can enhance both the electron transport and the high-energy ion population in the cathode plume. If ionization-driven modes also grow in the discharge then two more questions arise. Do these modes couple to the IAT and, if yes, how? Does operation in a Hall thruster affect this coupling differently than when the cathode is operated in a standalone arrangement? These questions cannot be fully answered without a first-principles, 2-D, time-dependent global model of the discharge that spans both the cathode interior and the plume/anode regions.

In this work we have employed for the first time the 2-D, time-dependent axisymmetric code OrCa2D to investigate the transition from spot to plume mode in a LaB_6 cathode developed and tested for HERMeS. In the cathode simulations $I_d/\dot{m}$ was increased by keeping I_d constant at 25 A while decreasing $\dot{m}$ from 20 sccm to 5 sccm. We find that the simulations capture the characteristic rise of $V_{k\text{-}pp}$ provided that the backpressure variation with cathode flow rate is accounted for; if the same backpressure is prescribed at all flow rates the amplitude of the oscillations is found much smaller than measured. The keeper voltage fluctuations at $\dot{m}<8$ sccm are found to be driven by oscillations in the plasma plume (of the same frequency) that increase in amplitude as the flow rate is reduced. By contrast, the plasma inside the cathode is found to be relatively quiescent. The oscillations are excited mostly in a region of the plume where the cathode neutral gas is fully depleted, and have a dominant frequency of <10 kHz. The plasma in this region is seen to undergo small longitudinal motions with wave velocity that is at least ~10× smaller than the drift, thermal and acoustic speeds of the ions. At 8 sccm the ionization frequency in the neutral-depleted plume region ranges ~2-100 kHz and equals the V_k oscillation frequency (of ~5 kHz) at the center of this region. The findings suggest that the transition to plume mode is indeed driven by ionization processes in the near-plume of the cathode, in line with previous conjectures from laboratory observations. Our results also underscore the significance of the plume neutral gas in this transition. We argue this also explains the dependence of the transition on the anode configuration since the latter affects directly the neutral gas density in the cathode plume. However, no simulations with different anode geometries have been performed yet to confirm this conjecture.

These first OrCa2D simulations establish a clear path towards the development of a global *ab initio* model of the transition from spot to plume mode. Along this path, additional simulations should be performed to demonstrate that other related observations made in the laboratory can be reproduced as well, such changes of the plume mode onset in the absence of an applied magnetic field, the effect of drawing current to (versus floating) the keeper, and the impact of different anode configurations, to name a few. Investigations into any coupling that may exist between ionization modes and IAT should be pursued as well to assess any implications on the generation of high-energy ions. Such studies however will require a more advanced model of the IAT growth than the saturation model of S&G used in this work.

Acknowledgments

The support of the joint NASA GRC and JPL development of HERMeS by NASA's Space Technology Mission Directorate through the Solar Electric Propulsion Technology Demonstration Mission (SEP TDM) project is gratefully acknowledged. The research described in this paper was carried out by the Jet Propulsion Laboratory, California Institute of Technology, under a contract with the National Aeronautics and Space Administration.

References

[1] E. V. Pawlik, and V. K. Rawlin, "A Mercury plasma-bridge neutralizer," *Journal of Spacecraft and Rockets,* vol. 5, no. 7, pp. 814-820, 1968/07/01, 1968.

[2] G. Csiky, "Investigation of a Hollow Cathode Discharge Plasma," *7th Electric Propulsion Conference*, International Electric Propulsion Conference: American Institute of Aeronautics and Astronautics, 1969.

[3] V. J. Friedly, and P. J. Wilbur, "High current hollow cathode phenomena," *Journal of Propulsion and Power,* vol. 8, no. 3, pp. 635-643, 1992/05/01, 1992.

[4] J. Brophy, and C. Garner, "Tests of high current hollow cathodes for ion engines," *24th Joint Propulsion Conference*, Joint Propulsion Conferences: American Institute of Aeronautics and Astronautics, 1988.

[5] D. M. Goebel, K. K. Jameson, I. Katz , and I. G. Mikellides, "Plasma Potential Behavior and Plume Mode Transitions in Hollow Cathode Discharge," in 30th International Electric Propulsion Conference, Florence, Italy, IEPC-2007-027, September 2007.

[6] A. Sengupta, J. Brophy, J. Anderson, C. Garner, B. Banks, and K. Groh, "An Overview of the Results from the 30,000 Hr Life Test of Deep Space 1 Flight Spare Ion Engine," *40th AIAA/ASME/SAE/ASEE Joint Propulsion Conference and Exhibit*, Joint Propulsion Conferences: American Institute of Aeronautics and Astronautics, 2004.

[7] J. Brophy, and C. Garner, "Tests of High-Current Cathodes for Ion Engines," in 24th AIAA/ASME/SAE/ASEE Joint Propulsion Conference, Boston,MA, AIAA-1988-2193, July 1988.

[8] D. M. Goebel, and I. Katz, *Fundamentals of electric propulsion : ion and Hall thrusters*, Hoboken, N.J.: Wiley, 2008.

[9] J. Brophy, D. Brim, J. Polk, and M. Henry, "The DS1 Hyper-Extended Mission " *38th AIAA/ASME/SAE/ASEE Joint Propulsion Conference and Exhibit*, Joint Propulsion Conferences: American Institute of Aeronautics and Astronautics, 2002.

[10] D. M. Goebel, K. K. Jameson, I. Katz, and I. G. Mikellides, "Potential fluctuations and energetic ion production in hollow cathode discharges," *Physics of Plasmas,* vol. 14, no. 10, Oct, 2007.

[11] D. M. Goebel, K. K. Jameson, I. Katz , I. G. Mikellides, and J. E. Polk, "Energetic Ion Production and Keeper Erosion in Hollow Cathode Discharges," in 29th International Electric Propulsion Conference, Princeton University, Princeton, NJ, IEPC-2005-266, October 2005.

[12] D. Goebel, I. Katz, R. Watkins, and K. Jameson, "Hollow Cathode and Keeper-Region Plasma Measurements Using Ultra-Fast Miniature Scanning Probes," *40th AIAA/ASME/SAE/ASEE Joint Propulsion Conference and Exhibit*, Joint Propulsion Conferences: American Institute of Aeronautics and Astronautics, 2004.

[13] B. A. Jorns, I. G. Mikellides, and D. M. Goebel, "Ion acoustic turbulence in a 100-A LaB_6 hollow cathode," *Physical Review E,* vol. 90, no. 6, Dec 5, 2014.

[14] A. Salhi, and P. Turchi, "A first-principles model for orificed hollow cathode operation," *28th Joint Propulsion Conference and Exhibit*, Joint Propulsion Conferences: American Institute of Aeronautics and Astronautics, 1992.

[15] M. Mandell, and I. Katz, "Theory of hollow operation in spot and plume modes," *30th Joint Propulsion Conference and Exhibit*, Joint Propulsion Conferences: American Institute of Aeronautics and Astronautics, 1994.

[16] M. P. Georgin, B. A. Jorns, and A. D. Gallimore, "An Experimental and Theoretical Study of Hollow Cathode Plume Mode Oscillations," in 35rd International Electric Propulsion Conference, Ann Arbor, MI, IEPC-2017-298, October 2017.
[17] I. G. Mikellides, I. Katz, D. M. Goebel, and K. K. Jameson, "Evidence of nonclassical plasma transport in hollow cathodes for electric propulsion," *Journal of Applied Physics,* vol. 101, no. 6, Mar 15, 2007.
[18] G. Sary, L. Garrigues, and J. P. Boeuf, "Hollow cathode modeling: II. Physical analysis and parametric study," *Plasma Sources Science & Technology,* vol. 26, no. 5, May 1, 2017.
[19] I. G. Mikellides, I. Katz, D. M. Goebel, and J. E. Polk, "Hollow cathode theory and experiment. II. A two-dimensional theoretical model of the emitter region," *Journal of Applied Physics,* vol. 98, no. 11, Dec 1, 2005.
[20] I. G. Mikellides, and I. Katz, "Wear mechanisms in electron sources for ion propulsion, 1: Neutralizer hollow cathode," *Journal of Propulsion and Power,* vol. 24, no. 4, pp. 855-865, Jul-Aug, 2008.
[21] I. G. Mikellides, I. Katz, D. A. Goebel, K. K. Jameson, and J. E. Polk, "Wear mechanisms in electron sources for ion propulsion, 2: Discharge hollow cathode," *Journal of Propulsion and Power,* vol. 24, no. 4, pp. 866-879, Jul-Aug, 2008.
[22] I. G. Mikellides, "Effects of viscosity in a partially ionized channel flow with thermionic emission," *Physics of Plasmas,* vol. 16, no. 1, Jan, 2009.
[23] J. Benjamin, M. G. Dan, and G. M. Ioannis, "Investigation of Energetic Ions in a 100-A Hollow Cathode," in 50th AIAA/ASME/SAE/ASEE Joint Propulsion Conference, Cleveland, OH, AIAA-2014-3826, July 2014.
[24] R. R. Hofer, J. E. Polk, M. J. Sekerak, I. G. Mikellides, H. Kamhawi, T. R. Sarver-Verhey, D. A. Herman, and G. Williams, "The 12.5 kW Hall Effect Rocket with Magnetic Shielding (HERMeS) for the Asteroid Redirect Robotic Mission," *52nd AIAA/SAE/ASEE Joint Propulsion Conference*, AIAA Propulsion and Energy Forum: American Institute of Aeronautics and Astronautics, 2016.
[25] D. A. Herman, W. Santiago, H. Kamhawi, J. E. Polk, J. S. Snyder, R. R. Hofer, and M. J. Sekerak, "The Ion Propulsion System for the Asteroid Redirect Robotic Mission," *52nd AIAA/SAE/ASEE Joint Propulsion Conference*, AIAA Propulsion and Energy Forum: American Institute of Aeronautics and Astronautics, 2016.
[26] S. B. Stanley, G. Chew, R. Rapetti, T. Tofil, D. A. Herman, M. Allen, B. Welander, J. Jackson, and R. Myers, "Development of a 13 kW Hall Thruster Propulsion System Performance Model for AEPS," *53rd AIAA/SAE/ASEE Joint Propulsion Conference*, AIAA Propulsion and Energy Forum: American Institute of Aeronautics and Astronautics, 2017.
[27] D. M. Goebel, and J. E. Polk, "Lanthanum Hexaboride Hollow Cathode Performance and Wear Testing for the Asteroid Redirect Mission Hall Thruster," *52nd AIAA/SAE/ASEE Joint Propulsion Conference*, AIAA Propulsion and Energy Forum: American Institute of Aeronautics and Astronautics, 2016.
[28] D. M. Goebel, K. K. Jameson, R. M. Watkins, I. Katz, and I. G. Mikellides, "Hollow cathode theory and experiment. I. Plasma characterization using fast miniature scanning probes," *Journal of Applied Physics,* vol. 98, no. 11, Dec 1, 2005.
[29] I. G. Mikellides, I. Katz, D. M. Goebel, J. E. Polk, and K. K. Jameson, "Plasma processes inside dispenser hollow cathodes," *Physics of Plasmas,* vol. 13, no. 6, Jun, 2006.
[30] I. G. Mikellides, D. M. Goebel, J. S. Snyder, I. Katz, and D. A. Herman, "The discharge plasma in ion engine neutralizers: Numerical simulations and comparisons with laboratory data," *Journal of Applied Physics,* vol. 108, no. 11, Dec 1, 2010.
[31] I. Katz, and I. G. Mikellides, "Neutral gas free molecular flow algorithm including ionization and walls for use in plasma simulations," *Journal of Computational Physics,* vol. 230, no. 4, pp. 1454-1464, Feb 20, 2011.

[32] A. L. Ortega, B. A. Jorns, and I. G. Mikellides, "Hollow Cathode Simulations with a First-Principles Model of Ion-Acoustic Anomalous Resistivity," *Journal of Propulsion and Power*, pp. 1-13, 2018.
[33] V. Y. Bychenkov, V. P. Silin, and S. A. Uryupin, "Ion-Acoustic Turbulence and Anomalous Transport," *Physics Reports-Review Section of Physics Letters,* vol. 164, no. 3, pp. 119-215, Jul, 1988.
[34] T. H. Stix, "Waves in Plasmas - Highlights from the Past and Present," *Physics of Fluids B-Plasma Physics,* vol. 2, no. 8, pp. 1729-1743, Aug, 1990.
[35] R. Z. Sagdeev, and A. Galeev, *Nonlinear plasma theory*, New York,: W. A. Benjamin, 1969.
[36] S. Dushman, "Electron emission from metals as a function of temperature," *Physical Review,* vol. 21, no. 6, pp. 0623-0636, Jun, 1923.
[37] P. Guerrero, I. G. Mikellides, and J. E. Polk, "Hollow cathode thermal modelling and self-consistent solutions. Work function evaluation for a LaB_6 cathode.," *54th AIAA/SAE/ASEE Joint Propulsion Conference*, AIAA Propulsion and Energy Forum: American Institute of Aeronautics and Astronautics, 2018.
[38] I. G. Mikellides, D. M. Goebel, B. A. Jorns, J. E. Polk, and P. Guerrero, "Numerical Simulations of the Partially Ionized Gas in a 100-A LaB_6 Hollow Cathode," *Ieee Transactions on Plasma Science,* vol. 43, no. 1, pp. 173-184, Jan, 2015.
[39] E. K. Storms, and B. A. Mueller, "Study of Surface Stoichiometry and Thermionic Emission Using Lab," *Journal of Applied Physics,* vol. 50, no. 5, pp. 3691-3698, 1979.
[40] J. G. Andrews, and R. H. Varey, "Sheath at an Electrode Close to Plasma Potential," *Journal of Physics, A: General Physics,* vol. 3, no. 4, pp. 413-420, 1970.
[41] J. Polk, C. Marrese, L. Dang, L. Johnson, and B. Thornber, "Temperature Distributions in Hollow Cathode Emitters," *40th AIAA/ASME/SAE/ASEE Joint Propulsion Conference and Exhibit*, Joint Propulsion Conferences: American Institute of Aeronautics and Astronautics, 2004.
[42] A. Lopez Ortega, I. G. Mikellides, and D. M. Goebel, "Numerical Simulations for Life Assessments of the BaO and LaB_6 Cathode Options in the Hall Effect Rocket with Magnetic Shielding (HERMeS)," in 35rd International Electric Propulsion Conference, Ann Arbor, MI, IEPC-2017-152, October 2017.
[43] I. G. Mikellides, I. Katz , K. K. Jameson, and D. M. Goebel, "Numerical Simulations of a Hall Thruster Hollow Cathode Plasma," in 30th International Electric Propulsion Conference, Florence, Italy, IEPC-2007-018, September 2007.
[44] B. A. Jorns, D. M. Goebel, and R. R. Hofer, "Plasma Perturbations in High-Speed Probing of Hall Thruster Discharge Chambers: Quantification and Mitigation," in 51st AIAA/SAE/ASEE Joint Propulsion Conference Orlando, FL, AIAA-2015-4006, July 2015, pp. 52.
[45] I. Mikellides, I. Katz, D. Goebel, and J. Polk, "Theoretical Modeling of a Hollow Cathode Plasma for the Assessment of Insert and Keeper Lifetimes," *41st AIAA/ASME/SAE/ASEE Joint Propulsion Conference & Exhibit*, Joint Propulsion Conferences: American Institute of Aeronautics and Astronautics, 2005.